Supporting Information for
Experimental and theoretical investigation of the Auger electron spectra of isothiocyanic acid, HNCS

Dorothee Schaffner,[a] Marius Gerlach,[a] Emil Karaev,[a] John Bozek,[b] Ingo Fischer,*[, a] Reinhold F. Fink*[, c]

September 24, 2024

[a] Institute of Physical and Theoretical Chemistry, University of Würzburg, 97074 Würzburg, Germany, ingo.fischer@uni-wuerzburg.de.
[b] Synchrotron SOLEIL, L'Orme des Merisiers, 91192 Gif-sur-Yvette, France.
[c] Institut für Physikalische und Theoretische Chemie, Universität Tübingen, Auf der Morgenstelle 18, 72076 Tübingen, Germany, reinhold.fink@uni-tuebingen.de

Contents

S1 Calculated structure of isothiocyanic acid **S2**

S2 Computational details **S2**

S3 X-Ray photoelectron spectra **S3**

S4 Comparison of HNCS and OCS Auger electron spectra **S6**

S5 Resonant Auger electron spectra **S7**

S6 Comparison of HNCS normal and resonant Auger electron spectra at the N1s edge **S9**

S7 References **S13**

S1 Calculated structure of isothiocyanic acid

The geometry and vibrational frequencies of the isothiocyanic molecule were calculated at the B3LYP/def2-TZVP level of theory. The calculated bond distances and bond angles are given in Table S1 and compare well with the experimental values from Yamada *et al.* which are also listed in Table S1.[1]

Table S1 Comparison of calculated and experimental[1] bond lengths and angles of the isothiocyanic acid molecule.

bond	calculated	experiment[1]
r(NH) /Å	1.005	0.9928
r(NC) /Å	1.200	1.2068
r(CS) /Å	1.569	1.5665
∢HNC /°	132.4	131.7
∢NCS /°	174.4	173.8

Calculated and experimental vibrational frequencies are listed in Table S2. The given assignment of the vibrational modes is adopted from Draper and Werner.[2] Our calculation however assigns the vibrational frequency at 650 cm^{-1} to an HNC bending mode and the one at 463 cm^{-1} to the in-plane NCS bending mode. The calculated wavenumbers show a good agreement with the experimental ones as well as with previous calculations of Wierzejewska and Moc at the B3LYP level of theory.[3]

Table S2 Comparison of calculated (unscaled) and experimental[2] vibrational frequencies of the isothiocyanic acid molecule.

calculated /cm^{-1}	experiment[2] /cm^{-1}	symmetry	assignment[2]
3666	3539	A′	ν(NH)
2045	1989	A′	ν_{as}(NCS)
881	857	A′	ν_{s}(NCS)
650	615	A′	δ(NCS)
494	539	A″	δ(NCS)
463	469	A′	δ(HNC)

S2 Computational details

The HNCS molecule was aligned such that the molecule lies in the *xy*-plane and the SC bond is parallel to the *x*-axis. Table S3 presents the molecular orbtial (MO) coefficients of the occupied Hartree-Fock orbitals of the HNCS molecule as well as the virtual valence orbitals that were generated according to the procedure described previously.[4] These virtual valence orbitals are orthogonal to the occupied orbitals and approximate eigenfunctions of its Fock-operator. That means, the combined orbital space of the occupied and virtual valence MOs is essentially equivalent to the orbital space of the occupied atomic orbitals (AOs) of the individual atoms within the molecule. Note, that more than 98 % of the occupied and virtual valence orbitals can be represented with the linear combination of the atomic valence orbitals in Table S3. This data shows that the core orbitals (1-6a′ and 1a″) are in an excellent approximation identical to the atomic ones. The valence orbitals (7-12a′ and 2-3a″) and the virtual valence orbitals (13a′ and 4a″) show significant contributions at the H 1s, N and C 2s and 2p as well as the S 3s and 3p atomic orbitals.

For core hole states the restricted open-shell Hartree-Fock (ROHF) procedure is severely plagued by poor convergence of the self-consistent field (SCF) iterations which frequently do not lead to the intended core-hole state. In order to ameliorate this limitation, we developed the following protocol. The initial guess for the MOs is obtained from the ground state Hartree-Fock MOs by identifying the orbital with the largest contribution of the respective core orbital, setting contributions of basis functions not belonging to the core hole atom to zero, and Schmidt orthogonalizing the other orbitals to this core MO. In the HF iterations, the coupling (nondiagonal Fock-type

Table S3 Molecular orbtial coefficients of the HNCS molecule in the single ζ-expansion of the molecular orbitals that was used for the evaluation of the Auger transition rates. The orbital energies ε are given in eV.

name	1a′	2a′	3a′	4a′	5a′	6a′	1a″	7a′	8a′	9a′	10a′	11a′	2a″	12a′	3a″	13a′	4a″
$-\varepsilon$	2502.36	424.62	309.88	243.94	180.86	180.79	180.78	34.87	28.55	22.32	16.61	15.56	15.40	10.56	10.13	−2.61	−3.86
$\sum_\mu c^2_{\mu,i}$	1.00	1.00	1.00	1.00	1.00	1.00	1.00	0.58	0.62	0.76	1.15	0.81	0.69	1.01	1.03	1.73	1.78
H 1s	0.00	0.00	0.00	0.00	0.00	0.00	0.00	0.06	−0.05	0.32	0.08	−0.01	0.00	−0.10	0.00	0.28	0.00
N 1s	0.00	1.00	0.00	0.00	0.00	0.00	0.00	−0.04	0.02	0.01	0.01	−0.02	0.00	0.01	0.00	−0.02	0.00
N 2s	0.00	0.00	0.00	0.00	0.00	0.00	0.00	0.63	−0.19	0.30	−0.09	−0.26	0.00	0.20	0.00	−0.25	0.00
N $2p_x$	0.00	0.00	0.00	0.00	0.00	0.00	0.00	0.05	−0.06	0.33	0.22	0.51	0.00	−0.44	0.00	0.43	0.00
N $2p_y$	0.00	0.00	0.00	0.00	0.00	0.00	0.00	−0.18	−0.04	0.52	0.05	−0.35	0.00	0.21	0.00	−0.28	0.00
N $2p_z$	0.00	0.00	0.00	0.00	0.00	0.00	0.00	0.00	0.00	0.00	0.00	0.00	0.59	0.00	−0.52	0.00	−0.72
C 1s	0.00	0.00	1.00	0.00	0.00	0.00	0.00	−0.06	−0.02	0.03	0.00	−0.01	0.00	0.01	0.00	−0.01	0.00
C 2s	0.00	0.00	0.00	0.00	0.00	0.00	0.00	0.31	0.32	−0.22	0.35	−0.01	0.00	−0.02	0.00	−0.07	0.00
C $2p_x$	0.00	0.00	0.00	0.00	0.00	0.00	0.00	0.02	−0.07	−0.02	0.05	0.47	0.00	0.17	0.00	−0.96	0.00
C $2p_y$	0.00	0.00	0.00	0.00	0.00	0.00	0.00	0.17	−0.37	−0.27	−0.41	0.14	0.00	−0.08	0.00	0.19	0.00
C $2p_z$	0.00	0.00	0.00	0.00	0.00	0.00	0.00	0.00	0.00	0.00	0.00	0.00	0.53	0.00	0.02	0.00	0.98
S 1s	1.00	0.00	0.00	0.00	0.00	0.00	0.00	0.00	−0.01	0.00	−0.01	0.00	0.00	0.00	0.00	0.00	0.00
S 2s	0.00	0.00	0.00	1.00	0.00	0.00	0.00	0.00	−0.06	−0.01	−0.06	0.03	0.00	0.00	0.00	0.00	0.00
S $2p_x$	0.00	0.00	0.00	0.00	0.23	0.97	0.00	0.00	−0.01	0.00	−0.01	−0.01	0.00	0.00	0.00	0.02	0.00
S $2p_y$	0.00	0.00	0.00	0.00	0.97	−0.23	0.00	0.00	−0.03	0.00	−0.03	0.01	0.00	0.00	0.00	0.00	0.00
S $2p_z$	0.00	0.00	0.00	0.00	0.00	0.00	1.00	0.00	0.00	0.00	0.00	0.00	−0.01	0.00	0.00	0.00	−0.02
S 3s	0.00	0.00	0.00	0.00	0.00	0.00	0.00	0.11	0.57	0.22	−0.74	0.21	0.00	−0.01	0.00	0.00	0.00
S $3p_x$	0.00	0.00	0.00	0.00	0.00	0.00	0.00	0.01	0.02	0.00	0.16	0.18	0.00	0.81	0.00	0.60	0.00
S $3p_y$	0.00	0.00	0.00	0.00	0.00	0.00	0.00	0.04	0.11	−0.04	0.46	−0.21	0.00	−0.17	0.00	−0.12	0.00
S $3p_z$	0.00	0.00	0.00	0.00	0.00	0.00	0.00	0.00	0.00	0.00	0.00	0.00	0.26	0.00	0.87	0.00	−0.53

matrix element) between the core orbital and the other orbitals is then reduced by a factor of five to ten in order to avoid that the character of the core orbital is changed too rapidly. During these iterations, reordering of the orbitals is switched off. The core-excited HF wave functions are obtained by adding a virtual orbital to the core-hole wave function with an improved virtual orbital or frozen core technique.[5–7] This provided sufficiently good start orbitals such that the ROHF procedure converges generally within about 20 iterations.

In order to guarantee smooth convergence of the core hole states for the ACPF and MCCEPA calculations, excitations of electrons which increase the number of electrons in the core hole shell were excluded.[8,9] For example, when the S$2p_x$ core hole state was described, we did not allow for excitations of electrons from any valence orbital into the S$2p_x$ hole. However, semiexternal double excitations which perform e.g. such an electron transfer combined with an excitation of an electron from the S$2p_y$ into a virtual orbital were included. It has been shown that such excitations are important to reproduce the proper character of the core hole states.[8]

S3 X-Ray photoelectron spectra

X-ray photoelectron spectra of isothiocyanic acid were recorded on the N1s, C1s, S2p and S2s edge and were used to determine the respective ionization energy (IE). In order to avoid post-collision interaction, a photon energy much higher than the ionization energy was used. In the X-ray photoelectron spectra (Fig. S1–S4) the binding energy is determined from the difference between the photon energy used and the measured kinetic energy. The spectra were calibrated with the help of N_2[10] (N1s edge), CO_2[11] (C1s edge) and Argon[12] (S2p and S2s edge) photolines.

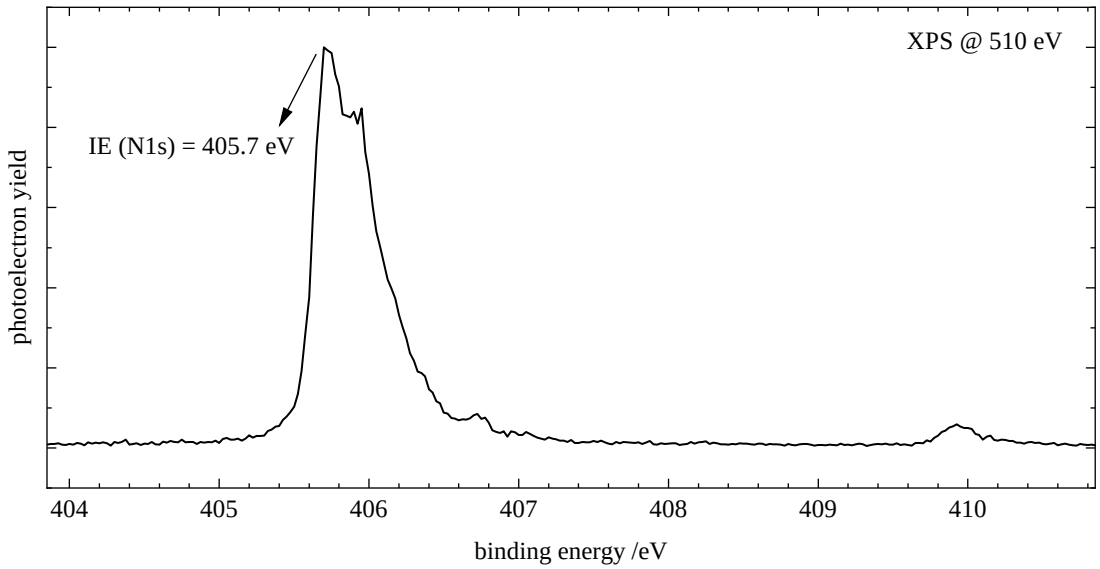

Fig. S1 : N1s X-ray photoelectron spectrum of HNCS measured at 510 eV. The N1s ionization potential was determined to be 405.7 eV. The shoulder at higher binding energies is presumably due to vibrational excitation. The signal at 406.7 eV is attributed to a HCN impurity from the synthesis. [13] At 409.9 eV a signal of molecular nitrogen is visible.

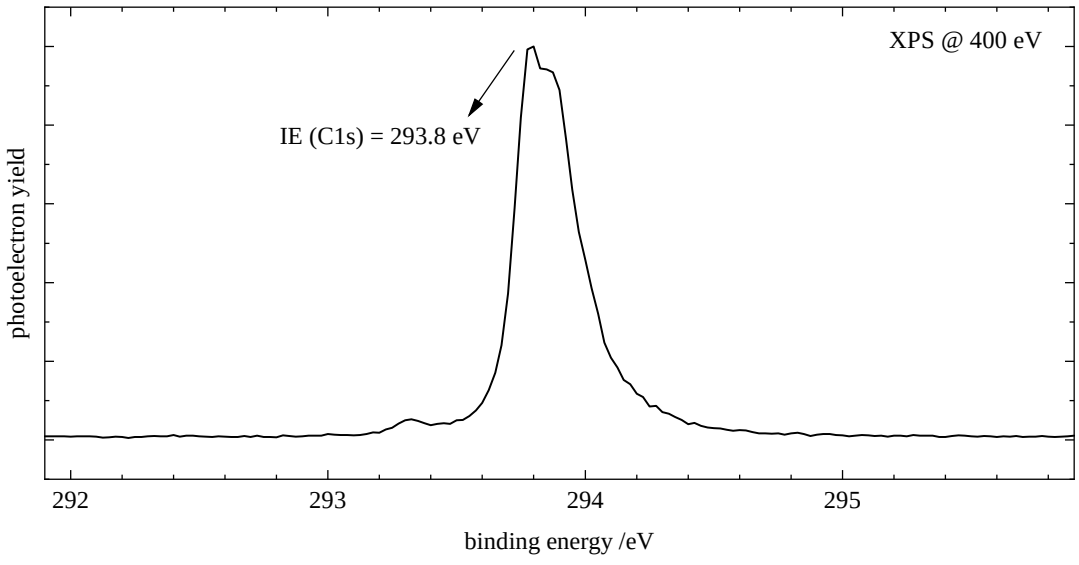

Fig. S2 : C1s X-ray photoelectron spectrum of HNCS measured at 400 eV. The C1s ionization potential was determined to be 293.8 eV. The shoulder at higher binding energies is presumably due to vibrational excitation. The signal at 293.3 eV is attributed to a HCN impurity from the synthesis. [13]

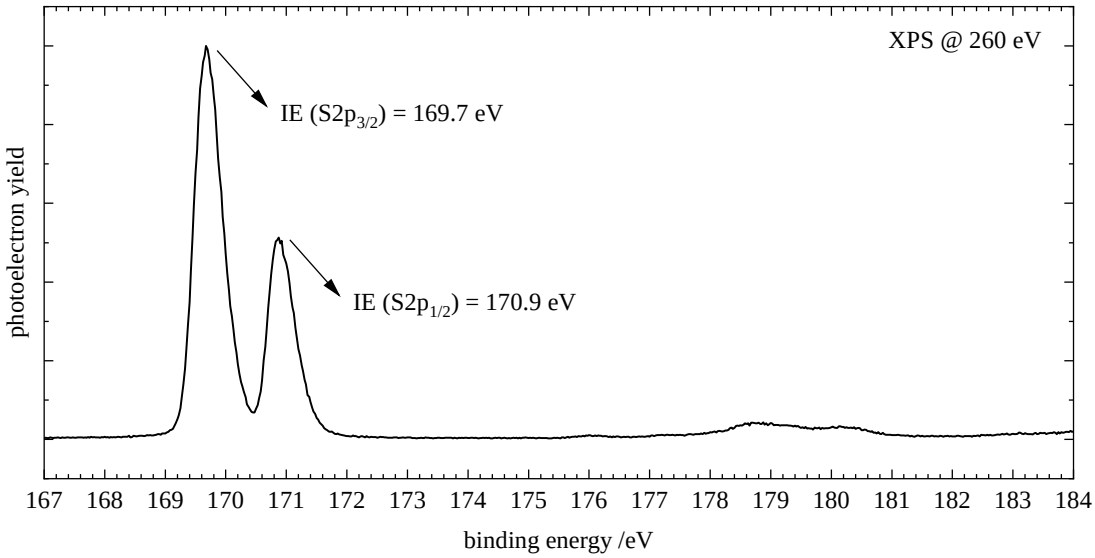

Fig. S3 : S2p X-ray photoelectron spectrum of HNCS measured at 260 eV. The spin-orbit coupling of the S2p shell leads to separated $S2p_{3/2}$ and $S2p_{1/2}$ peaks with an intensity ratio of 2:1 and a splitting of 1.2 eV. The $S2p_{3/2}$ ionization potential was determined to be 169.7 eV while the $S2p_{1/2}$ ionization potential is 170.9 eV. The smaller signals around 179 eV possibly are shake-up satellites, where another electron is excited into a virtual orbital.

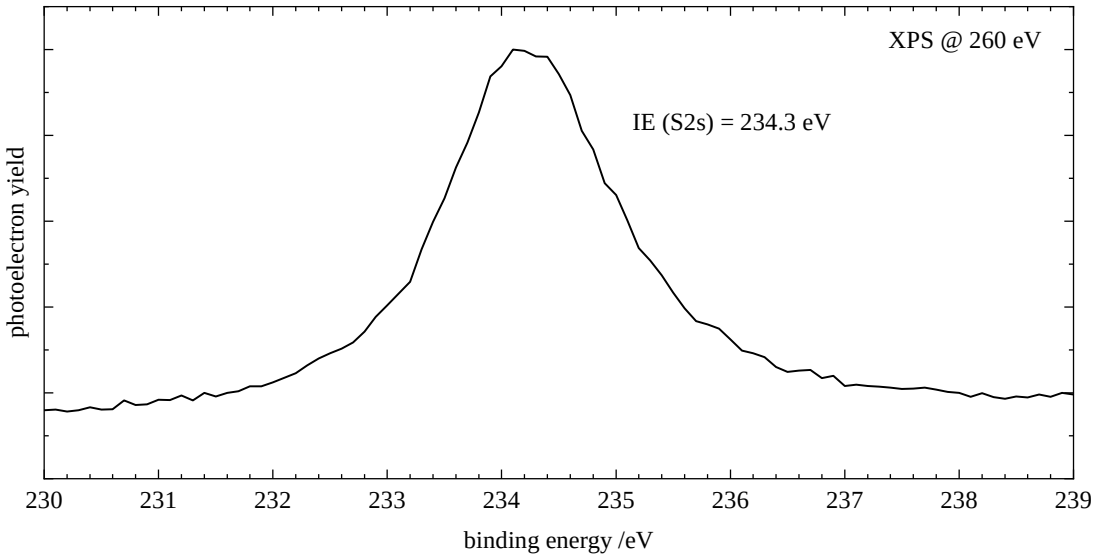

Fig. S4 : S2s X-ray photoelectron spectrum of HNCS measured at 260 eV. The S2s ionization potential was determined to be 234.3 eV. From the Lorentzian part of the fit to a Voigt profile a lifetime width of 1.72 eV was determined (see main paper). Small deviations from a perfectly symmetric line profile could be due to PCI effects that influence the line shape and which were not considered for the determination of the lifetime width.

S4 Comparison of HNCS and OCS Auger electron spectra

Isothiocyanic acid can be compared to the isosteric molecule carbonyl sulfide, OCS, where the NH unit is replaced by an oxygen. As described in section 3.1 in the main paper the ground state configuration of HNCS is: (core) $7a'^2 8a'^2 9a'^2 10a'^2 11a'^2 2a''^2 12a'^2 3a''^2$. The ground state configuration of the linear OCS molecule is (core) $6\sigma^2 7\sigma^2 8\sigma^2 2\pi^4 9\sigma^2 3\pi^4$.[14] While the OCS molecule possesses two sets of doubly degenerate π-orbitals, 2π and 3π, their degeneracy is lifted when going from the linear to the bent geometry in HNCS. From the MO scheme in Fig. 1 in the main paper we identify the sets of formerly degenerate orbitals as 11a′, 2a″ and 12a′, 3a″. The 9σ orbital of OCS corresponds to the 10a′ orbital of HNCS. The Auger electron spectra of OCS have been investigated both experimentally and theoretically[14–16] and we expect similarities in the spectra of the two molecules. Their spectra are shown in Fig. S5, note that we compare the HNCS N1s edge to the OCS O1s edge. All spectra of OCS were shifted to lower energies by 3 eV to account for the difference in electronegativity between oxygen and nitrogen. The labelling of the features corresponds to the one in Fig. 2 in the main paper. In all cases, the shape of the spectra is similar, although the intensities are different.

In HNCS the feature up to 31 eV is assigned to the decay to final states with occupations that reveal vacancies in the HOMO and

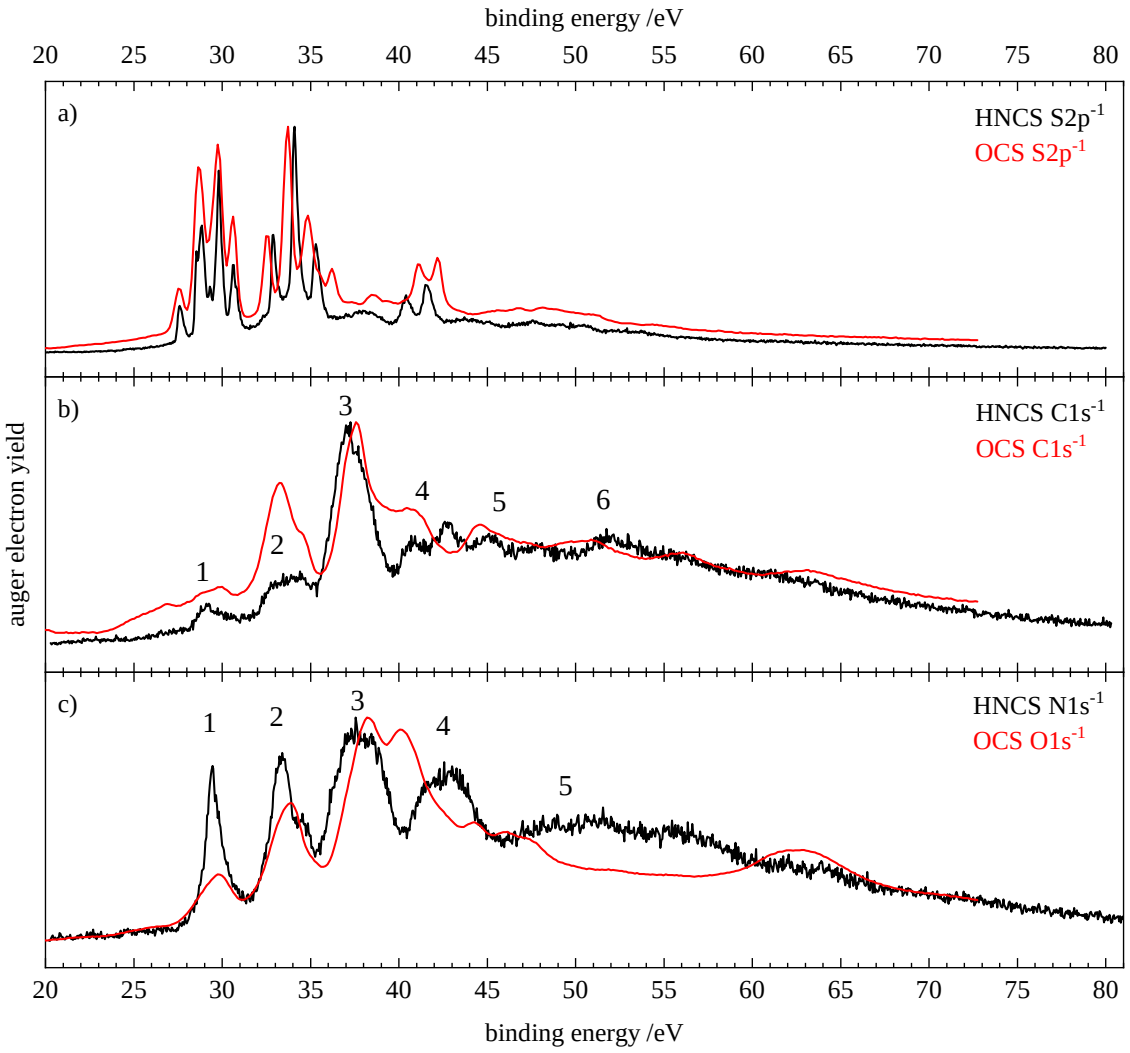

Fig. S5 Comparison of the normal Auger electron spectra of isothiocyanic acid (black) and carbonyl sulfide (red). The spectra of carbonyl sulfide were each shifted by 3 eV to lower binding energy. Carbonyl sulfide spectra were reprinted from Ref. 15 with permission from Elsevier.

HOMO-1 (12a′ and 3a″). This is consistent with the assignment of the corresponding feature in OCS as decay to final states with $(3\pi)^{-2}$ occupation. On the sulfur edge we observe a similar splitting into a multiplet with four components for both molecules. As in HNCS the low binding energy signal in OCS is assigned to a transition of the S2p$_{1/2}$ component to a triplet final state while singlet final states and the respective S2p$_{3/2}$ component contribute to the signals at higher binding energies.[14] For HNCS the low intensity of feature 1 on the carbon edge is rationalized by the low contribution of the C2p atomic orbital to the molecular orbitals involved in the decay, 12a′ and 3a″. A similar behaviour is observed for OCS due to the nodal plane of the 3π orbital on the carbon atom.

The assignment of the feature from 32–35 eV in the Auger electron spectra of HNCS is in accordance with the one found for OCS although differences in the relative intensity are present and the second multiplet on the sulfur edge in OCS reveals four instead of three bands as in HNCS. In OCS a main contribution of final states described by $2\pi^{-1}3\pi^{-1}$ orbital occupations (corresponding to $(2a''/11a')^{-1}(12a'/3a'')^{-1}$) is found for the carbon and oxygen edge, while the decays S2p$_{1/2}$/S2p$_{3/2}\rightarrow{}^3\Pi$, $^1\Pi$ with $9\sigma^{-1}3\pi^{-1}$ and $8\sigma^{-1}3\pi^{-1}$ occupation dominate on the sulfur edge.[14] The final states found on the S2p edge in HNCS correspond to a $9\sigma^{-1}3\pi^{-1}$ occupation.

In the 35–40 eV region the higher intensity on the carbon and nitrogen edge of HNCS (feature 3) compared to the sulfur edge is explained with the shape of the molecular orbitals involved in the decay. According to our calculations these molecular orbitals, 2a″ and 11a′, are mainly located on the carbon and nitrogen atom. This explanation is confirmed by the comparison to OCS where a similar phenomenon is observed as the 2π orbital shows the highest density on the carbon and oxygen atom.[15]

At higher binding energies of 40–45 eV the doublet on the S2p edge of HNCS compares well with the one found for OCS. Our assignment to ^{1}A′(10a′$^{-2}$) and ^{1}A′(9a′$^{-1}$10a′$^{-1}$) final states corresponds to the description as final states with $9\sigma^{-2}$ and $8\sigma^{-1}9\sigma^{-1}$ occupation in OCS.[14,16] A comparison of the N1s edge to the O1s AES of OCS shows that the spectra differ profoundly at higher binding energies. Especially the band at 40 eV in the OCS spectrum, which is attributed to $8\sigma^{-1}2\pi^{-1}$ final states, is not found for HNCS. This difference contrasts with the similarity at the S2p edge of OCS and HNCS, but is not surprising, because the sulfur atom is hardly influenced by substituting the oxygen by an isosteric NH unit.

S5 Resonant Auger electron spectra

Figure S6 shows the resonant spectra as well as the off-resonant spectrum that were recorded at the C1s edge. The excitation energies are indicated in the C1s NEXAFS spectrum in Fig. 4 b) in the main paper. The resonant Auger electron spectra exhibit similar features at all excitation energies, however differences in the resonant enhancement and the band shapes are observed. The photon energy of 286.59 eV corresponds to the low-energy side of the C1s $\rightarrow$ 13a′ excitation and the following five traces to the excitation of the different vibrational levels (v = 0–4) of the C1s^{-1}13a′^{1} core excited state. All corresponding RAES show a resonant enhancement of the features at 13.5, 15.2 eV and >18 eV, whereby the most intense band broadens which indicates decays to higher vibrational levels of the 2a″$^{-1}$ and 11a′$^{-1}$ final states due to changes in the Franck-Condon overlap of the core excited and final state when higher vibrational levels are excited. Changes on the high-energy part of the lowest participator band and of the band at 15.2 eV also indicate transitions between different vibrational levels of the intermediate and final state. The C1s $\rightarrow$ 4a″ excitation (287.73–288.01 eV) leads to a stronger enhancement of the band at 13.5 eV and the scan over this excitation reveals only very subtle changes in the RAES. The excitation of the resonance at 290.66 eV also shows an enhancement of the same band and a very high intensity of the spectator region that strongly resembles the normal C-AES. This implies that the spectating electron is excited to virtual orbitals located far away from the molecule as in case of a Rydberg state.

The resonant spectra as well as the off-resonant spectrum that were recorded at the N1s edge are presented in Figure S7. The

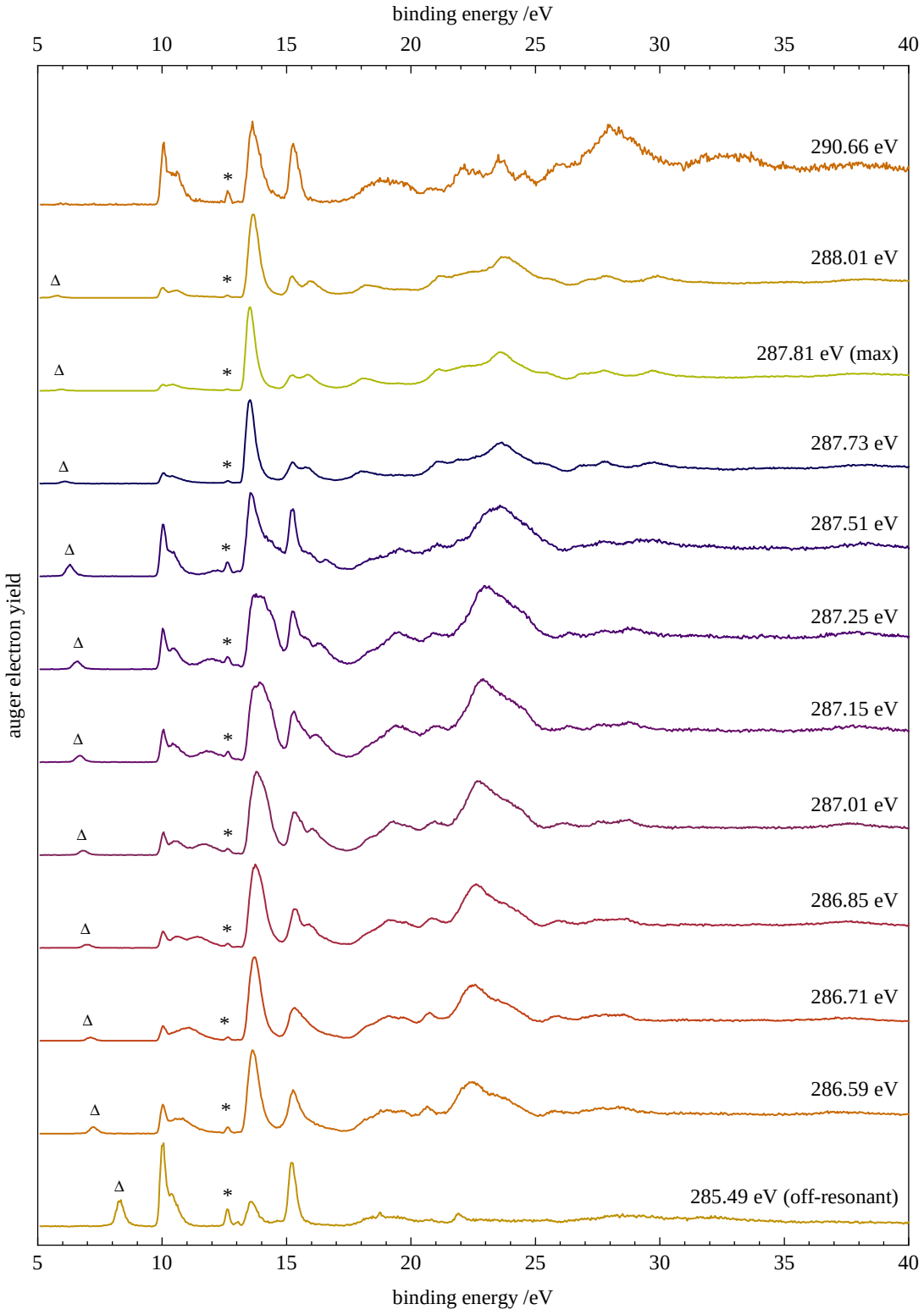

Fig. S6 : Resonant Auger electron spectra of isothiocyanic acid at the carbon 1s edge and off resonant spectrum. The spectra were recorded at the excitation energies indicated in the C1s NEXAFS spectrum in Fig. 4 b) in the main paper. Asterisks at 12.62 eV indicate a signal of water. The bands indicated by triangles are due to carbon 1s ionisation by second harmonic light.

excitation energies are indicated in the N1s NEXAFS spectrum in Fig. 4 c) in the main paper. As the NEXAFS signal at 407.19 eV does not belong to a resonance of HNCS the spectrum measured at this photon energy is not shown. However this spectrum can be found in Fig. S9. As mentioned in the main paper we observe a resonant enhancement of the band at 15.2 eV for both 13a′ and 4a″ excitation. At the high energy side of the N1s $\rightarrow$ 4a″ resonance intensity modulations in the high energy part of the feature at 10 eV imply interference effects of different vibrational levels. Excitation of the higher core excited state at 401.8 eV enhances the participator line at 13.5 eV whose asymmetric shape hints unresolved vibrational structure of the underlying participator final states. Two narrow spectator transitions are observed at 19.8 and 23.7 eV. This could indicate final states of a very similar geometry to the core excited state. For the excitation at even higher photon energies the spectator region's similarity to the normal AES at the nitrogen edge increases as observed on the carbon edge.

Figure S8 shows the resonant spectra as well as the off-resonant spectrum that were recorded at the S2p edge. The excitation energies are indicated in the S2p NEXAFS spectrum in Fig. 4 a) in the main paper and belong to a superposition of $S2p_{1/2}$ and $S2p_{3/2}$ excitations into different virtual orbitals. For the transitions into low-lying core excited states we observe an enhancement of the band at 15.2 eV and of the spectator region, which dominates the RAES at higher excitation energies and exhibits very distinct features. In the spectator region of the RAES measured at the highest resonant excitation energy (169.46 eV) we observe the normal Auger electron spectrum of only one of the spin-orbit split S2p components.

Upon excitation at 165.42, 165.68 and 165.90 eV we observe a small, sharp signal at higher binding energies which is marked by an arrow in Fig. S8. These signals correspond to a constant kinetic energy of 136.5 eV. A constant kinetic energy as a function of photon energy indicates an ultrafast dissociation of the core-excited molecule due to a dissociative core-excited state. The signal at a kinetic energy of 136.5 eV corresponds to the Auger-Meitner decay of a core-excited atomic sulfur fragment ($S2p^5 3s^2 3p^5$) to S^+ $^2D_{3/2,\,5/2}$ ($2p^6 3s^1 3p^4$). The core-excited atomic fragment could be produced in its $^3D_3$ or $^1P_1$ state, for which kinetic energies of 136.66 or 136.44 eV are expected. These values are based on the cationic final state that was found to lie 22.50 eV higher in energy than the neutral ground state[17] and on calculated energies for the core-excited states of 159.16 eV ($^3D_3$) and 158.94 eV ($^1P_1$) relative to the neutral ground state.[18] For OCS an atomic line at the same kinetic energy of 136.5 eV is observed in the resonant Auger electron spectrum upon S2p $\rightarrow$ 10σ* excitation.[18] From the comparison of atomic contributions to the X-ray fluorescence spectrum and the resonant Auger electron spectrum the atomic sulfur line was attributed to the S $^3D_3 \rightarrow S^+$ $^2D_{3/2,\,5/2}$ transition.

S6 Comparison of HNCS normal and resonant Auger electron spectra at the N1s edge

In order to estimate the screening effect of the spectating electron we compare the resonant Auger electron spectra at the nitrogen edge (lower traces) to the normal Auger electron spectrum (upper trace) on a kinetic energy scale in Fig. S9. Here we also include the spectrum measured at 407.19 eV above the ionization threshold (resonance of N_2). The energy difference between the first band in the normal Auger electron spectrum (2h state) and the first spectator state (2h1p state) in the resonant spectra is equal to the screening effect of the spectating electron and is given as horizontal arrows in Fig. S9. The core electron that is resonantly excited shields the emitted Auger electron from the nuclear charge which results in a higher kinetic energy (lower binding energy). As expected for the excitation into the close-lying 13a′ (LUMO) and 4a″ (LUMO+1) orbitals we observe a similar screening effect which amounts to 7.7 eV. This is roughly 1 eV lower compared to HNCO, where a screening effect of about 9 eV is found.[19] Excitation into higher core excited states gradually reduces the screening and for the excitation at 404.52 eV we observe only a value of 1.7 eV. This implies that the spectating electron is located far away from the nucleus and the excited state is therefore likely to be of Rydberg character. Due to the less tightly bound spectating electron the coupling between the double valence hole and the spectating electron in 2h1p final states is

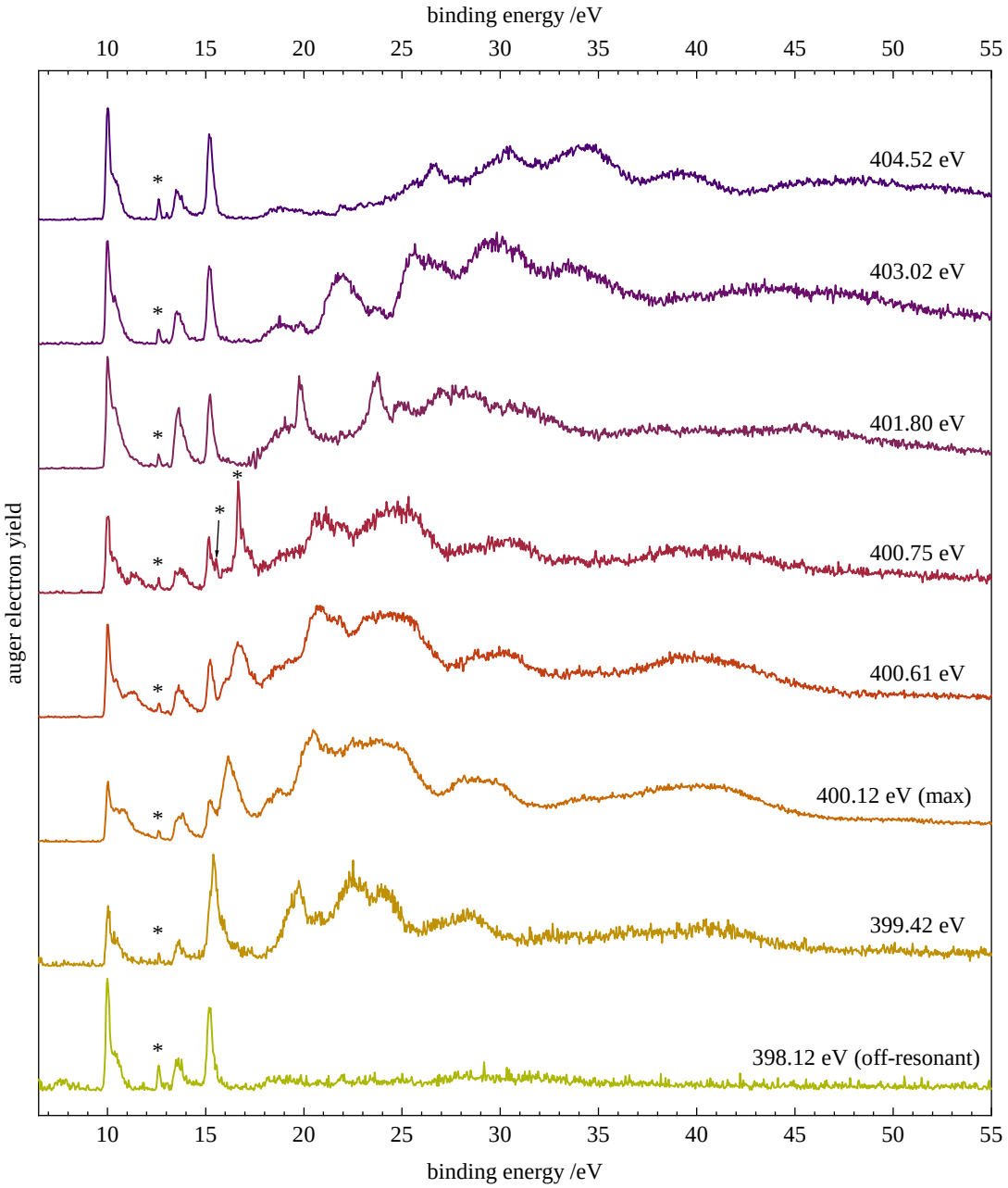

Fig. S7 : Resonant Auger electron spectra of isothiocyanic acid at the nitrogen 1s edge and off resonant spectrum. The spectra were recorded at the excitation energies indicated in the N1s NEXAFS spectrum in Fig. 4 c) in the main paper. The spectra at 400.61 and 401.80 eV were corrected for signals from a molecular nitrogen impurity by subtracting a pure N_2 spectrum that was measured at the same photon energy. Asterisks at 12.62 eV mark a signal of water, while additional asterisks in the spectrum at 400.75 eV indicate signals from N_2.

reduced which results in spectator transitions that very much resemble the parent Auger lines in the normal AES.

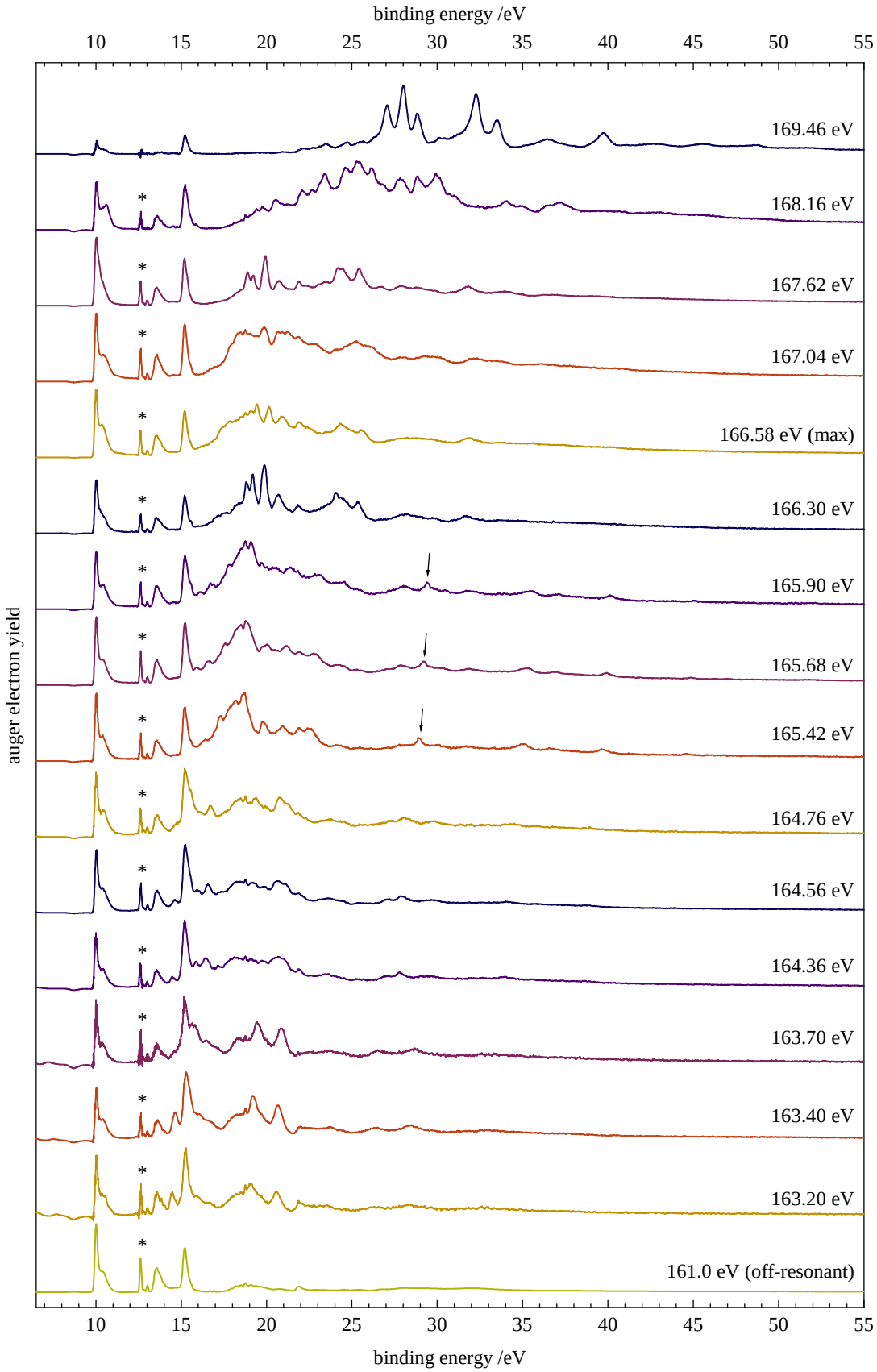

Fig. S8 : Resonant Auger electron spectra of isothiocyanic acid at the sulfur 2p edge and off resonant spectrum. The spectra were recorded at the excitation energies indicated in the S2p NEXAFS spectrum in Fig. 4 a) in the main paper. Asterisks at 12.62 eV indicate a signal of water. Black arrows mark signals from sulfur that is produced by ultrafast dissociation. As mentioned in the main paper we corrected the resonant spectra for the contribution from direct photoemission by subtraction of a scaled off resonant spectrum.

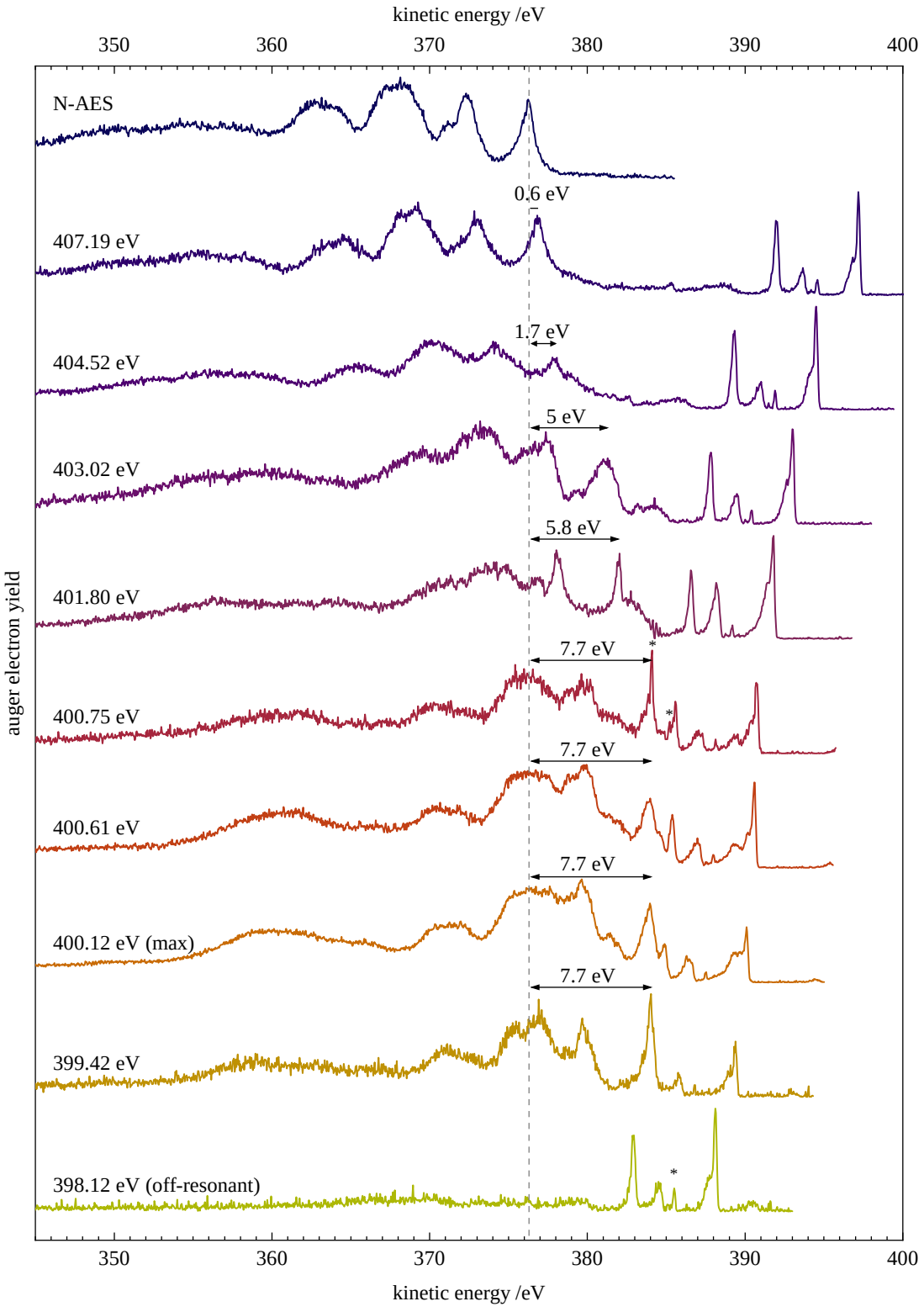

Fig. S9 : Normal (upper trace) and resonant (lower traces) Auger electron spectra of isothiocyanic acid at the nitrogen 1s edge in kinetic energy. Horizontal arrows indicate the value of the screening effect. The spectra at 400.61 and 401.80 eV were corrected for signals from a molecular nitrogen impurity by subtracting a pure N_2 spectrum that was measured at the same photon energy. The asterisk in the off-resonant spectrum marks a signal of water, while additional asterisks in the spectrum at 400.75 eV indicate signals from N_2.

S7 References

References

1 K. Yamada, M. Winnewisser, G. Winnewisser, L. B. Szalanski and M. C. L. Gerry, *J. Mol. Spectrosc.*, 1980, **79**, 295–313.

2 G. R. Draper and R. L. Werner, *J. Mol. Spectrosc.*, 1974, **50**, 369–402.

3 M. Wierzejewska and J. Moc, *J. Phys. Chem. A*, 2003, **107**, 11209–11216.

4 R. F. Fink, S. L. Sorensen, A. Naves de Brito, A. Ausmees and S. Svensson, *J. Chem. Phys.*, 2000, **112**, 6666–6677.

5 D. Demoulin and M. Jungen, *Theor. Chim. Acta*, 1974, **34**, 1–17.

6 J. Wasilewski, *Int. J. Quantum Chem.*, 1991, **39**, 649–656.

7 N. Rossler and V. Staemmler, *Phys. Chem. Chem. Phys.*, 2003, **5**, 3580–3586.

8 K. J. Børve, *Chem. Phys. Lett.*, 1996, **262**, 801–806.

9 R. F. Fink, M. Kivilompolo, H. Aksela and S. Aksela, *Phys. Rev. A*, 1998, **58**, 1988.

10 G. Johansson, J. Hedman, A. Berndtsson, M. Klasson and R. Nilsson, *J. Electron Spectrosc. Relat. Phenom.*, 1973, **2**, 295–317.

11 V. Myrseth, J. D. Bozek, E. Kukk, L. J. Sæthre and T. D. Thomas, *J. Electron Spectrosc. Relat. Phenom.*, 2002, **122**, 57–63.

12 G. C. King, M. Tronc, F. H. Read and R. C. Bradford, *J. Phys. B: At. Mol. Phys.*, 1977, **10**, 2479.

13 A. Giertz, K. J. Børve, M. Bäßler, K. Wiesner, S. Svensson, L. Karlsson and L. J. Sæthre, *Chem. Phys.*, 2002, **277**, 83–90.

14 D. Minelli, F. Tarantelli, A. Sgamellotti and L. S. Cederbaum, *J. Chem. Phys.*, 1997, **107**, 6070–6079.

15 T. X. Carroll, D. Ji and T. D. Thomas, *J. Electron Spectrosc. Relat. Phenom.*, 1990, **51**, 471–486.

16 P. Bolognesi, P. O'Keeffe and L. Avaldi, *J. Phys. Chem. A*, 2009, **113**, 15136–15141.

17 W. C. Martin, R. Zalubas and A. Musgrove, *J. Phys. Chem. Ref. Data*, 1990, **19**, 821–880.

18 R. F. Fink, A. Eschner, M. Magnuson, O. Björneholm, I. Hjelte, C. Miron, M. Bassler, S. Svensson, M. N. Piancastelli and S. L. Sorensen, *J. Phys. B: At., Mol. Opt. Phys.*, 2006, **39**, L269.

19 F. Holzmeier, T. J. A. Wolf, C. Gienger, I. Wagner, J. Bozek, S. Nandi, C. Nicolas, I. Fischer, M. Gühr and R. F. Fink, *J. Chem. Phys.*, 2018, **149**, 034308.